Can small events (M<0) observed during hydraulic fracture stimulations initiate large events (M>0)?

Adam Baig, Ted Urbancic, Gisela Viegas, and Sepideh Karimi, Engineering Seismology Group

It is becoming evident that under different circumstances, such as injection rates and geologic conditions, it might be possible to generate large magnitude (M > 0) events during hydraulic fracture stimulations. By utilizing fully integrated passive seismic monitoring programs, we can examine the relationship between the occurrence of small magnitude events (M < 0) and the fracture and stress conditions that may lead to larger events. In our investigations, we identify that over all scales of observation the events follow a self-similar behavior; however, the small magnitude events are generally lower in stress release than observed for the larger events. These differences can be explained by the observed failure mechanisms where smaller events tend to be driven by shear-tensile failures of pre-existing discrete fractures (joints) whereas the larger events appear to be dominated by shear-driven failure processes associated with pre-existing faults. These observations suggest that there can be sufficient stress transfer and stress build up resulting from the smaller events associated with hydraulic stimulation to allow for nearby pre-existing faults to slip in shear.

Introduction

Typically, the monitoring of hydraulic fracture stimulations is carried out with high-frequency geophones temporarily placed close to reservoir depth. Inherent with these arrays are bandwidth limitations that limit the size distribution of observed fractures to failures associated with pre-existing joint sets or asperities/barriers associated with larger faults. To accurately portray the discrete fracture network, recording with supplementary low-frequency geophones or accelerometers can be used to extend the observed fracture size distribution to include larger coalesced fracture or fault sizes. Capturing the various size scales provides opportunities to more completely identify activated structures during hydraulic fracture stimulations. The overall distribution of fracture sizes with magnitude, often referred to as scaling relations, can be closely examined for differences or similarities in behavior, namely whether size distributions follow models of constant stress drop. Departures from self-similarity may be related to source and/or site effects, such as the presence of lower driving stresses resulting from fluids in the development of fracture zones as compared to shear-stress-driven failures commonly associated with faults.

By incorporating multisensor array networks distributed around the stimulation volume, both at surface and downhole, we can also identify the components of failure using advanced seismic signal analysis techniques, namely seismic moment tensor inversion (SMTI). By utilizing these approaches we can identify, for example, the failure type, such as mixed-mode shear/tensile failure associated with a rough fracture surface, the fluid flow pathways and enhanced fluid flow

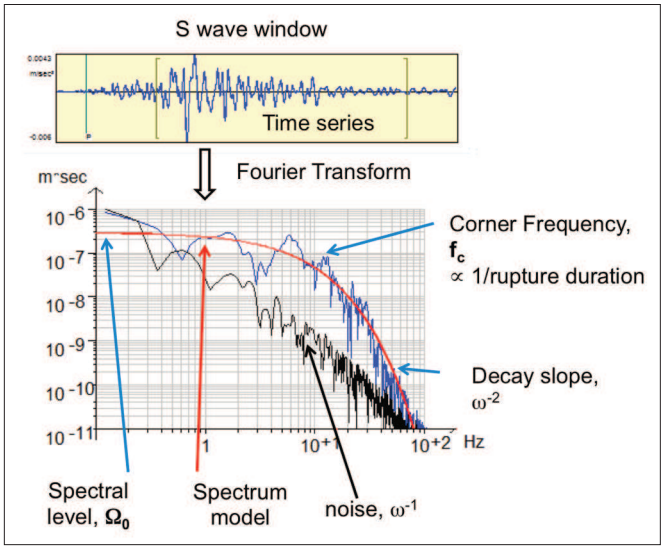

Figure 1. *Attenuation-corrected amplitude-displacement source spectrum of a seismic event (S-wave = blue line) and pre-event noise (black line). The two asymptotes used in its approximation are represented by a Brune model fit as a red line. The usable frequency bandwidth is in the range where signals are not dominated by noise (~ 0.7–40 Hz).*

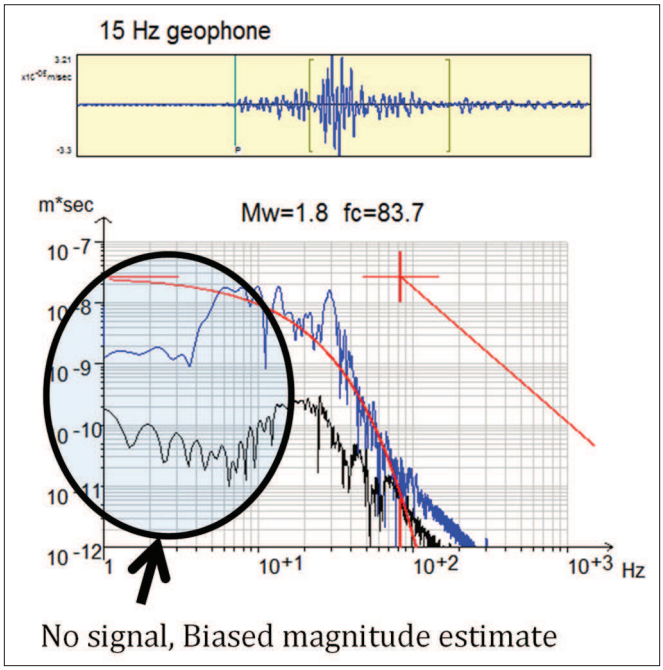

Figure 2. *Rotated S-wave from the same event shown in Figure 1 as observed recorded with a 15-Hz geophone at reservoir depth and its attenuation-corrected amplitude-displacement source spectrum. As indicated by the circle, depleted signals at low frequencies due to bandwidth and signal limitations can bias the moment estimates, and result in an underestimation of the event magnitude. Additionally, at higher frequencies, around 350 Hz, signals are contaminated by resonance effects and lower signal-to-noise, further resulting in limited recording bandwidth.*

volume as related to the relative degree of open fractures, and the distribution of fracture lengths (power law distribution). We can further relate the observed fractures to identified pre-existing fracture and fault networks, and the stress behavior leading to fracture activation, be it either stimulation-induced or due to stress transfer effects. This then provides a pathway to characterizing the conditions leading to the potential occurrence of large-magnitude events (M > 0) associated with stimulations.

In this paper, we discuss the potential of using data recorded utilizing both near-surface three- component force balance accelerometers, 4.5-Hz geophones, and downhole 15-Hz geophones to assess the conditions under which hydraulic fracture stimulations can initiate large events (M > 0). This analysis includes comparing the scaling behavior of larger-magnitude events as compared to the scaling exhibited by smaller events, and identifying their failure mechanisms as a possible underlying explanation for any observed differences in scaling behavior. Correlations between observed scaling behaviors and mechanisms then allow for the speculation as to whether stress changes, stress build-up and stress-transfer mechanisms are sufficient to result in observed large-magnitude event occurrences.

Instrumentation, instrument types, and the importance of full-scale coverage

Seismic events inherently are band-limited becasue of the nature of the generation process and their source failure mechanisms. The dominant frequencies generated for these events are related to the stopping phase of the rupture, which can then be related to the source dimensions (source radius) and the amplitude associated with the dominant frequency can be related to the source size (magnitude) of the event. This results in band-limited frequency content that can be considered characteristic of the particular event size being generated.

In the frequency domain, the displacement-amplitude source spectrum of a seismic event can be modeled or approximated by two asymptotes (Figure 1): one horizontal asymptote in the low-frequency part of the spectrum, and an inclined asymptote following the ω^{-2} falloff of the higher frequencies (Brune, 1970). The frequency corresponding to the point where the two asymptotes intersect is referred to as the corner frequency and is inversely proportional to the rupture duration. Larger events will have higher-amplitude low-frequency asymptotes and smaller corner frequencies (or longer rupture duration) assuming the rupture velocity and stress drop (stress release) are the same. Attenuation can severely hamper high frequencies, changing the shape of the source spectrum. The asymptote following the high-frequency falloff will have an increased slope (slope < ω^{-2}) and the corner frequency will shift to a lower apparent corner frequency. To correct for attenuation, it is assumed that the increased slope is due to attenuation and can be corrected by applying a Q correction to retrieve a ω^{-2} slope.

To properly characterize and interpret the behavior of these events, appropriate instrumentation and sampling rates need to be utilized to maximize the usable bandwidth of the signals. For example, downhole monitoring of microseismic data (M<0) during hydraulic fracturing and other fluid-injection programs typically incorporates 15-Hz elements, which, in theory when shunted, provide a flat response (to within 3 dB) from about 15 Hz up to about 1000 Hz. However, these elements are not the only part of the overall recording system, which also consists of the sensor pod, a cable (usually wireline) that suspends the pods, a mechanism to couple the pods to the wellbore, the coupling of the wellbore to the Earth, and the digitizing/recording units. Each component introduces noise into the observed signal that can erode signal quality and thereby result in limiting the usable bandwidth. In the best-case scenario, the overall recording system yields an undistorted picture of ground motion from 15 Hz to the Nyquist frequency as imposed by the digitizer or the high-frequency limit of the sensor (around 1000 Hz). More often, recording conditions translate into resonances ranging from about 350–750 Hz, which, along with limitations due to the event-generation process, results in a usable bandwidth ranging from about 80–350 Hz (Figure 2). These signals can be further eroded due to attenuation effects and poor signal-to-noise ratios. As a result, only when these recording effects are taken into account can the appropriate analysis of recorded signals be considered.

To enhance bandwidth detection limits and increase the size scale recording range, the use of 15-Hz sensors needs to be augmented with low-frequency sensors such as force balance accelerometers (FBAs) and the use of low frequency 2 or 4.5-Hz sensors which can provide bandwidth coverage from about 0.5–100 Hz. These sensors generally are used to increase the size scale to include events with M > 0 and typically are installed close to or at the surface. Aside from issues that arise that are similar to downhole acquisition, installation effects such as ground conditions and proximity to the surface

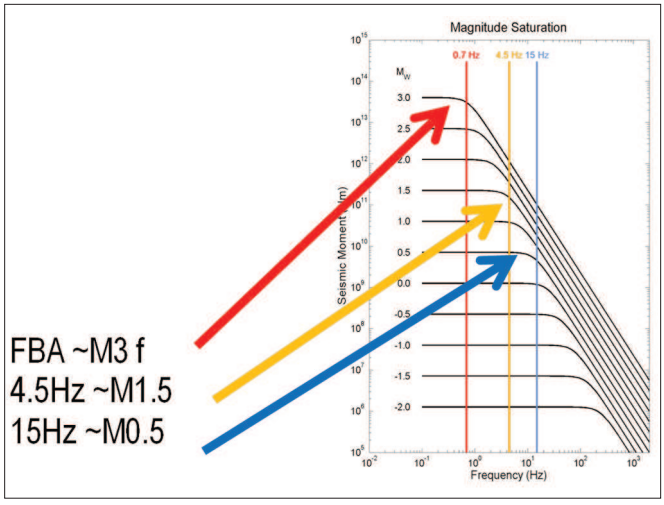

Figure 3. *Synthetic source spectra of –M2 to M3 events (assumed stress drop of 0.1 MPa) and lower-frequency band limit of geophones and FBA. Saturation of the magnitude scale occurs when the long-period spectral plateaus fall completely outside the recording bandwidth (that is when the event corner frequency is below the natural frequency of the recording instrument).*

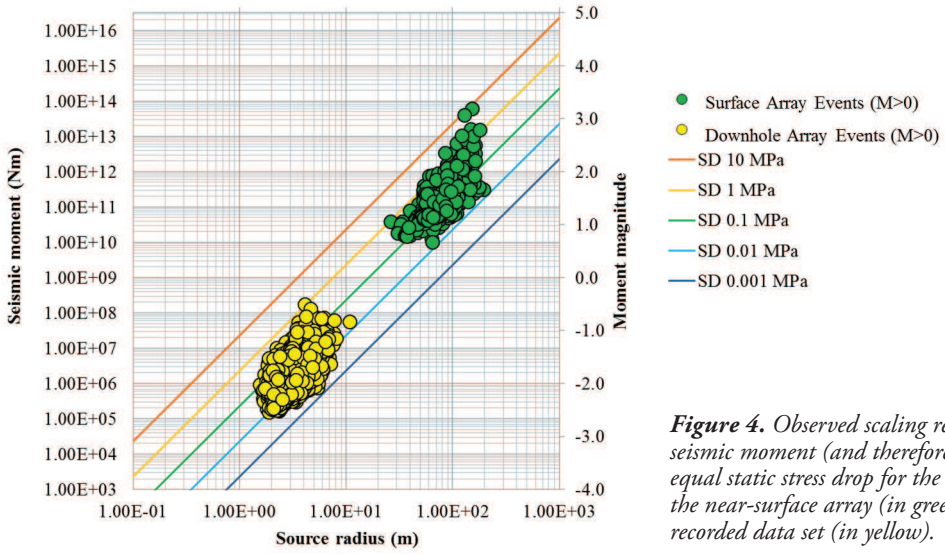

Figure 4. *Observed scaling relations between source radius and seismic moment (and therefore moment magnitude), with lines of equal static stress drop for the larger-magnitude events detected with the near-surface array (in green) and smaller-magnitude downhole-recorded data set (in yellow).*

have a profound effect on the observed signals. When higher-frequency geophones are used to characterize the spectrum from events with corner frequencies below the bandwidth of the sensor, the low-frequency plateau critical to describing the spectrum of the waveforms will be missing and the source parameters will be unreliable, dominated by saturation effects (also refer to Figure 2). In Figure 3, we estimate (for events with a constant stress drop) at which magnitudes these saturation effects create limitations on signal interpretation for different sensors (Viegas et al., 2012).

For the data sets discussed below, we consider data recorded downhole and close to the surface (within 50 m) in order to provide for effective monitoring of induced seismicity ranging in magnitude from $-4 < M < +4$. The combination of instrumentation also reduces possible magnitude-saturation issues and frequency band limitations and their influence on scaling behavior.

Scaling relations

Examining the scaling behavior of events of different sizes has long been considered as a way to predict the behavior of larger events as extrapolated from the observed scaling of smaller magnitude events. By considering how event seismic moment scales with the source radius and utilizing Brune's penny-shaped crack fault model, we can identify whether events follow a self-similar behavior (follow lines of constant stress drop) or nonsimilar behavior (increasing seismic moment with constant source radius). In either case, the analysis through spectral analysis has to account for bandwidth limitations, propagation, and site effects before underlying differences can be explained in terms of source behavior.

Numerous examples in the literature have looked into scaling behavior. For hard-rock excavation-induced events, nonsimilar scaling relationships have been observed for weakly structured rock masses with reduced clamping stresses, whereas self-similar behavior has been found for heavily fractured zones under stress confinement (Urbancic et al., 1993). Overall, the interaction of stresses with pre-existing fractures and fracture complexity, initially thought as a second-order effect, appears to significantly influence source characteristics of excavation induced seismic events with $M < 0$ and consequently favors a nonsimilar earthquake generation process. It has also been considered that excavation-induced events contain a significant volumetric component of failure and as such result in significantly lower stress drops as compared to pure shear sources. For reservoir-induced events, it has been shown that these events typically have on average ten times lower stress drops than natural tectonic earthquakes, suggesting that reservoir-induced seismicity can occur with a lower stress drop due to the high pore pressures of the underground medium (Goertz-Allmann et al., 2011). Similarly, in hydraulic fracture stimulations, lower average stress drops have also been reported and have thought to be related to heterogeneous slip along less well-developed or previously nonexistent fractures. (Fehler and Phillips, 1991).

Data: M>0 surface-detected events versus M<0 downhole-detected events.

For the purposes of this paper, we discuss a data set consisting of events recorded during hydraulic fracture stimulations at a depth of approximately 1.6 km. Around 1000 events with $M > 0$ were detected from a modest network of near-surface stations during a multiple well completion of a single pad over a period of a few weeks. To properly characterize the positive magnitudes that can be easily observed from a distance of 1.6–5 km; each station consisted of a force balanced accelerometer deployed with a 4.5-Hz geophone. A number of these events were also detected on a seismometer that was part of a national network about 100 km from the site of the event. The downhole events, which were recorded in the same field but over a different time interval, comprise one stage of data from the completion of a lateral well, and were monitored from a number of wells around the stage of interest. For this stage, over 400 events were located. For both sets of events, we calculated source characteristics such as seismic moment, magnitude, source radius, energy release, and stress

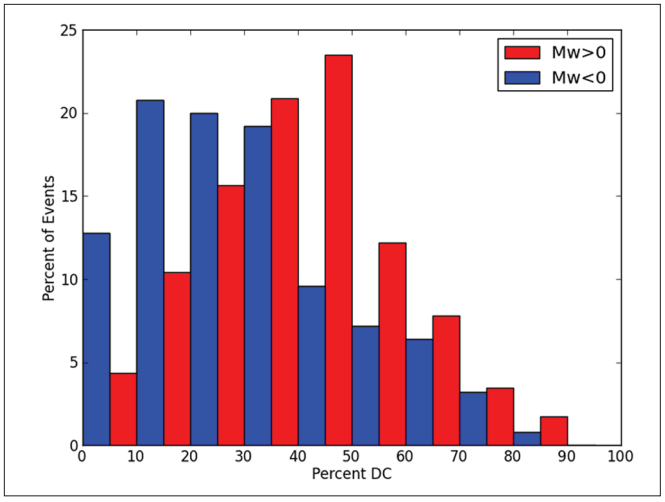

Figure 5. *Histogram comparing the percentage contribution from the double-couple component from both the surface-recorded Mw > 0 and downhole Mw < 0 data sets.*

release utilizing a time-domain spectral equivalent approach. Additionally, to indicate whether the event mechanisms can be determined, all events were assessed for condition number; those events with a good condition number were used in the determination of failure components through moment tensor inversion (to be discussed further in the following section).

The relationships between moment and source radius are plotted against lines of constant stress drop for the data sets considered in Figure 4. Although there is some scatter, each individual data set appears to follow a self-similar distribution, as shown by their tendency to follow lines of constant stress drop. However, the two data sets are not self-similar with each other, as the average stress drop for the smaller-magnitude events detected downhole is about an order of magnitude lower than the large-magnitude events observed from the near surface. This observation suggests that the generating mechanisms for these data are fundamentally different.

Seismic moment tensor inversion

In order to investigate the differences in source behavior, we take advantage of the favorable source-array geometries in the data sets to do seismic moment tensor inversion. The mechanisms for the events are directly related to the radiation patterns of *P*- *SV*-, and *SH*-waves. Observations of these waveforms from a distribution of sensors that sufficiently span the volume allows for the amplitudes and polarities of these phases to be back-projected along raypaths back to the focal sphere, reconstructing the radiation patterns. In practical terms, this provision on sensor geometry for downhole observation of microseismic events usually translates to the need for the signals to be detected across multiple receiver arrays deployed in nearby wells. For surface or near-surface monitoring of larger-magnitude seismicity, this restriction is not practically as strict. So long as waveforms are observed from a sufficient number of azimuths, the moment tensor can be robustly determined.

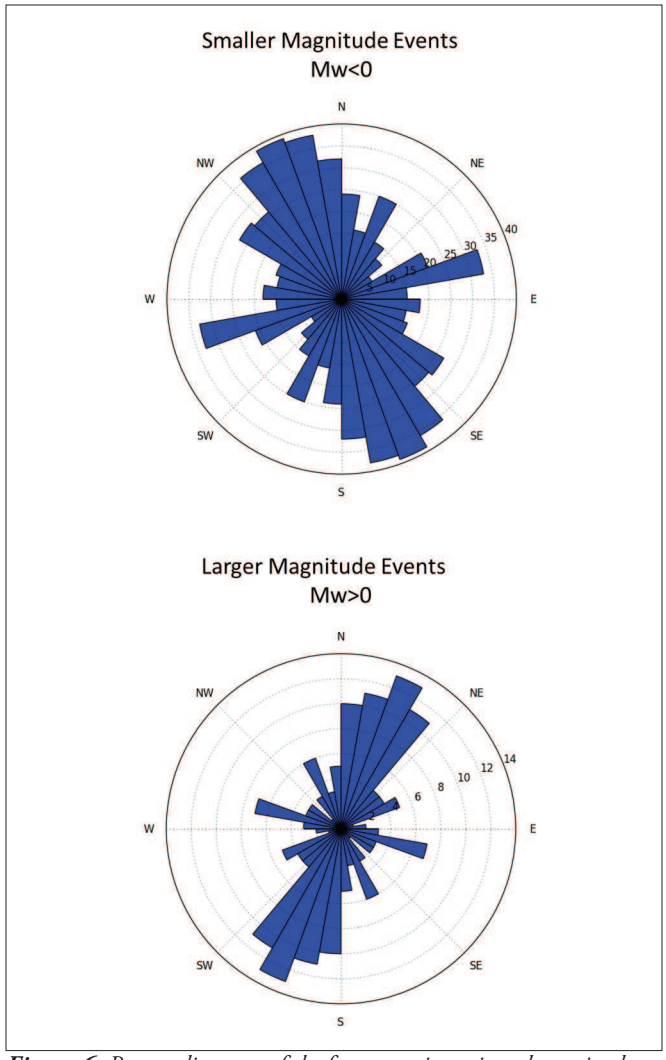

Figure 6. *Rosette diagrams of the fracture orientations determined from the two data sets.*

The moment tensor is proportional to the instantaneous strain and as such can be described by a symmetric 3 × 3 matrix of force couples. Because of the symmetry, it has six independent components. These six components can be rearranged into one component describing the size of the event (i.e., the moment or moment magnitude), three components describing the orientations of the orthogonal strain axes, and two components that describe the style of the deformation. These two components describe deviations from double couple (DC) mechanisms: one is the isotropic component which describes the volumetric increase or descrease of the source region and the other is the compensated linear vector dipole (CLVD) component, where strain along one axis (outward or inward) is compensated by opposing strain (i.e., inward or outward, respectively).

Additionally, for fracture-related events, the orientations of the strain axes can be related to the orientation of the fractures. For double-couple events, this particular problem has been the subject of much attention in the geophysical literature since any particular DC moment tensor results in two equally valid solutions. In order to resolve this ambiguity, a

group of related DC events can be inverted for a best-fitting state of stress, which will make one solution more likely than the other. The situation is much simpler for events closer to opening and closures, as the fracture planes for these cases will be normal to the outward and inward strain axes, respectively.

Discussion

For these data, we plot the contributions of the double-couple component to the different mechanisms associated with both the smaller-magnitude events from the downhole monitoring and the larger-magnitude events from the surface monitoring (Figure 5). There is a very notable shift in the style of the mechanisms between the downhole and surface data sets, in that the larger-magnitude data have in general a much stronger shear component. The lower-magnitude data have much smaller shear associated with them, suggesting that slip is not a dominant mechanism in these events, in line with the opening and closing mechanisms observed during hydraulic fracture stimulations (see Baig and Urbancic, 2010). These differences in behavior further suggest that a mechanistic difference exists between the event source sizes and could be the underlying reason as to why the differences in scaling behavior are observed.

Rosette diagrams for the orientations of the fracture planes are a convenient way of showing the dominant fracture orientations. As shown in Figure 6, the large-magnitude events tend to follow a single consistent orientation, favorably oriented to the maximum horizontal stress in the region of NE-SW. The fracture orientations for the smaller events are more varied and are dominated by movement along the pre-existing fracture network as identified through core and downhole imaging data. These data further suggest that the downhole-recorded data are activating different features than the data seen on the near-surface arrays.

Based on these results, we can speculate on the underlying process responsible for the observations. The prevalence of double-couple-dominant events for the larger-magnitude events is indicative of stress-driven processes that are generating these events. The smaller-magnitude events, showing significant deviations from double couple, necessitate fluid involvement in the failure process. Furthermore, although the larger- and smaller-magnitude data sets are themselves self-similar, these events follow different scaling-relations paths. The events themselves are responding to different generating mechanisms, the smaller events, tensile in nature, are the likely the response of the joint sets and other lineations in the reservoir to the fluid injection. The events of larger magnitude that are seen from the near-surface network are necessarily activating larger-scale features, greater than 100-m source radii. These features are likely pre-existing faults, previously unidentified, in the formations at and below the reservoir. In general, these differences can be explained by the observed failure mechanisms where smaller events tend to be driven by shear-tensile failures of pre-existing discrete fractures (joints) whereas the larger events appear to be dominated by shear-driven failure processes associated with pre-existing faults. The occurrence of large events is likely related to a stress transfer resulting from the stress changes or transfer resulting from the occurrence of smaller-magnitude events in the volume. Based on these observations, we suggest that there is a sufficient stress transfer and stress buildup resulting from the smaller events to allow for pre-existing faults to slip in shear. The presence of these faults, that can be activated by the stress-shedding effects during hydraulic fracture treatments, can have profound effects on the understanding of the fracture propagation in the reservoir and create potential pathways that can lead to either enhanced or ineffective stimulations. TLE

References

Aki, K. and P. G. Richards, 2002, Quantitative seismology: Theory and methods: University Science Books.

Anderson, J. G. and S. Hough, 1984, A model for the shape of the Fourier amplitude spectra of accelerograms at high frequencies: Bulletin of the Seismological Society of America, **74**, 1969–1994.

Baig, A. M., T. I. Urbancic, and G. Viegas, 2012, Do hydraulic fractures induce events large enough to be felt on surface?: CSEG Recorder, 10, 40–46.

Brune, J. N. , 1970, Seismic source dynamics: Supplement to Reviews of Geophysics, 29, 688-699.

Fehler, M. and W. S. Phillips, 1991, Simultaneouins version for Q and source parameter of microearthquakes accompanying hydraulic fracturing in granitic rock: Bulletin of the Seismological Society of America, **81**, 553–575.

Goertz-Allmann, B. P., A. Goertz, and S. Wiemer, 2011, Stress drop variations of induced earthquakes at the Basel geothermal site: Geophysical Research Letters, **38**, L09308, doi:10.1029/2011GL047498.

Hough, S. E., L. Seeber, A. Lerner-Lam, G. Armbruster, and H. Guo, 1991,. Empirical Green's function analysis of Loma Prieta aftershocks: Bulletin of the Seismological Society of America, **81**, 1737–1753.

Urbancic, T. I., B. Feignier, and R. P. Young, 1993, Influence of source region properties on scaling relations for M < 0 events: Pure and Applied Geophysics, **139**, 721–739.

Viegas, G., A. Baig, W. Coulter, and T. Urbancic, 2012, Effective monitoring of reservoir-induced seismicity utilizing integrated surface and downhole seismic networks: First Break, **30**, 77–81.

Corresponding author: adam.baig@esgsolutions.com